

Article

Analysis of Wind-Turbine Main Bearing Loads Due to Constant Yaw Misalignments over a 20 Years Timespan

Martin Cardaun , Björn Roscher , Ralf Schelenz and Georg Jacobs

Center for Wind Power Drives, RWTH Aachen University, 52062 Aachen, Germany; bjoern.roscher@cwd.rwth-aachen.de (B.R.); Ralf.Schelenz@cwd.rwth-aachen.de (R.S.); georg.jacobs@imse.rwth-aachen.de (G.J.)

* Correspondence: martin.cardaun@cwd.rwth-aachen.de

Received: 20 March 2019; Accepted: 8 May 2019; Published: 10 May 2019



Abstract: The compact design of modern wind farms means that turbines are located in the wake over a certain amount of time. This leads to reduced power and increased loads on the turbine in the wake. Currently, research has been dedicated to reduce or avoid these effects. One approach is wake-steering, where a yaw misalignment is introduced in the upstream wind turbine. Due to the intentional misalignment of upstream turbines, their wake flow can be forced around the downstream turbines, thus increasing park energy output. Such a control scheme reduces the turbulence seen by the downstream turbine but introduces additional load variation to the turbine that is misaligned. Within the scope of this investigation, a generic multi body simulation model is simulated for various yaw misalignments. The time series of the calculated loads are combined with the wind speed distribution of a reference site over 20 years to investigate the effects of yaw misalignments on the turbines main bearing loads. It is shown that damage equivalent loads increase with yaw misalignment within the range considered. Especially the vertical in-plane force, bending and tilt moment acting on the main bearing are sensitive to yaw misalignments. Furthermore, it is found that the change of load due to yaw misalignments is not symmetrical. The results of this investigation are a primary step and can be further combined with distributions of yaw misalignments for a study regarding specific load distributions and load cycles.

Keywords: wake steering; yaw misalignment; multi body simulation; main bearing loads; rain flow counts

1. Introduction

Wind turbines are mainly clustered as wind farms. Due to the limited space, the turbines are densely placed to obtain the full potential of the available space and to avoid unnecessary cabling costs especially at offshore sites. The turbine in the wake flow experiences lower wind speeds and increased turbulence intensity [1]. As a result maximizing the output of the individual turbine does not always lead to a global maximum wind farm output. Furthermore, the increased turbulence intensity leads to greater loads on the drive train and its structural components [1]. This results in accelerated damage accumulation and shortened maintenance intervals. However, there are two approaches to reduce these effects.

During power curtailment the power of an upstream turbine is reduced. This means that the wind speed in the wake is less reduced. Therefore, more power can be extracted by the downstream turbines. However, the turbine in the wake still experiences an increased turbulence intensity. This control scheme was the topic of a significant amount of research, see [2–5].

Wake-steering offers a promising approach. The upstream turbines are misaligned against the inflow direction, which directs the wake flow past the downstream turbine. Simulations showed that the average power capture could be increased by such a control scheme, see [6,7]. In [8] the simulation results were compared with real park measurements and the increase in energy capture matched the predicted values. Further, in [9] it was shown that a wind farm already optimized with respect to wake losses could increase its annual energy supply by up to 3.7% through the use of wake steering. In addition the non-torque loads of the downstream turbine are reduced because of the lower turbulence intensity as shown in [10,11]. In [12,13], the power output and blade root moments of the waked turbine were measured. It was found that the turbine power drops significantly when the yaw misalignment exceeds 10° . Furthermore, a correlation between the yaw angle and flapwise bending moment was made. In [14] aerodynamic loads were compared between measurement and simulation. The results showed that aerodynamic loads could be calculated accurately, even for highly yawed inflows. With respect to these results, a significant influence of the yaw misalignment on bending and tilt moment at the main bearing is expected. Therefore, this study will address the torque and non-torque loads at the main bearing of the turbine in the front that is misaligned.

The main contribution of this work is the structure focussed approach. Many studies regarding wake-steering focus on the flow field and the ones that take the structure into account mostly observe the blade root moments. In this study, the transmission of the aerodynamic loads into the drive train and support structure of the turbine are studied as a function of the yaw misalignment. The work is limited in its consideration of the flow field since the Blade-Element-Momentum Theory is used to calculate the wind loads on the rotor blades instead of a complex CFD simulation which would be necessary to study the flow around the blade profiles. Because of that, the yaw angle is limited to a range of -10° to $+10^\circ$ due to the limitation of the utilised code. As an initial classification of the occurring load changes and the detection of further effects, load calculations are carried out on a generic wind turbine model with flexible structural components. For this purpose, a multi body simulation model of a 3 MW turbine with a rotor diameter of 126 m ($C3 \times 126$ [15]) is simulated at Design Load Case 1.1 according to DIN EN 61400-1 (production operation) [16] with wind class 2B at multiple yaw misalignments. The loads at the main bearing are investigated, since this is where changes in the aerodynamic loads by an inclined flow will mainly be reflected and, for the most part, be introduced into the structure. The resulting understanding can be used both in the design process and in operation. On the one hand, the findings could be taken into account in the design of the bearings, and on the other hand, the park regulation could be adapted to prevent an uneconomical accumulation of damage in favour of energy production.

2. Simulation Model and Setup

Within the scope of this work the resulting turbine loads are determined by a co-simulation between SIMPACK, AERODYN [17] and MATLAB. The multi body simulation software SIMPACK Version 2019 is used to formulate the mechanical structure of the turbine including flexible tower and blades. The AERODYN-code delivers the aerodynamic loads acting in the blades and the controller of the turbine is formulated in MATLAB. For a wind speed below the rated wind speed the turbine is controlled by a generator torque and the above rated wind speed the turbine is pitch-controlled. The drive train of the turbine is modelled as a 2-mass-oscillator with equivalent stiffness and inertia to a gearbox with a ratio of 92.28. Relevant turbine parameters can be found in Table 1. The turbine delivers power in a wind speed range from $v_{hub} = 3$ m/s to $v_{hub} = 25$ m/s (wind speed on hub height in front of the rotor). For this range, three-dimensional turbulent wind fields are generated in steps of 1 m/s with TurbSim [18]. According to the design load case (DLC) 1.1 of the industry standard DIN EN 61400-1 [16], wind fields of wind class 2B are generated with a normal turbulence model ($I_{ref} = 0.14$). The standard deviation of the longitudinal wind speed at the hub height results from Equation (1). The inflow data is arranged in a matrix representing a grid in front of the rotor. For each point on the

grid the wind speed data for all three dimensions is stored as a time series. The frequency of the time series is 20 Hz.

$$\sigma_1 = I_{ref}(0.75 v_{hub} + b); b = 5.6 \text{ m/s} \quad (1)$$

Table 1. C3 × 126 turbine parameters [15].

Variable	Value	Unit
Rated power	3.0	MW
Tower height	112.0	m
Rotor diameter	126.0	m
Hub height	115.0	m
Cut-in wind speed v_{in}	3.0	m/s
Cut-out wind speed v_{out}	25.0	m/s
Rated wind speed v_{rated}	11.0	m/s
Tilt angle	6	°
Gearbox ratio	1:92.28	-
Main suspension	3-Point	-

The loads due to yaw misalignments of -10° , -5° , 0° , $+5^\circ$ and $+10^\circ$ are investigated within the scope of this work. The potential weaknesses of the methodology are as follows. The Blade-Element-Momentum Theory doesn't take the interaction between the neighbouring blade elements into account. In addition, it neglects the wake expansion. Since a detailed examination of the flow field around the blades is not intended in this work, these assumptions will have a negligible influence on the results. The used AERODYN-Code utilizes the Blade-Element-Momentum Theory with Glauert Correction for yawed rotors [19], so the simulation is not valid beyond the chosen yaw angle values. However, the overall effects and trends resulting from the misalignment will be detectable within the chosen yaw angle range. In addition, there are the structural assumptions that were made to model the rotor blades which are built as shell elements. The natural frequencies of the flexible blades and tower are considered up to 11 Hz. This ensures that the most important deformations can be mapped but also allows for manageable computation times. For the blades, bending modes up to the first order and torsional modes up to the fourth order are considered. The tower model includes bending modes up to the fifth order and the torsional mode of the first order.

Figure 1 shows the nacelle position relative to the wind direction. The multi body simulation model of the entire turbine is also shown in Figure 1. A simulation of 10 min is performed at each wind speed. The calculated loads are then cumulated over a period of 20 years. The wind speeds are weighted with respect to the probability of their occurrence. The cumulative frequencies of the wind speeds result from the reference location described in the German renewable energies act (EEG 2017) [20]. The height profile of the wind is calculated according to the Hellmann power law with a Hellman exponent of $\alpha = 0.25$ and the reference wind speed and reference hub height (Equation (2); $v_{ref} = 6.45 \text{ m/s}$, $h_{ref} = 100 \text{ m}$). This results in the mean wind speed at hub height with $v_{Hub} = v(h = h_{Hub})$. Using the mean wind speed at hub height v_{Hub} , the cumulative frequencies are to be determined by a Rayleigh distribution (Equation (3)). In order to determine the relative frequency of the respective wind speed, the difference of the sum frequencies of v_i and v_{i-1} is calculated (Equation (3)). The distribution of the relative frequencies is shown in Figure 2. Identical wind fields are used for the load calculation of each yaw misalignment.

$$v = v_{ref} \left(\frac{h}{h_{ref}} \right)^\alpha \quad (2)$$

$$F(v_i) = 1 - \exp \left[-\frac{\pi}{4} \left(\frac{v_i}{v_{hub}} \right)^2 \right] \quad (3)$$

$$H(v_i) = F(v_i) - F(v_{i-1}) \quad (4)$$

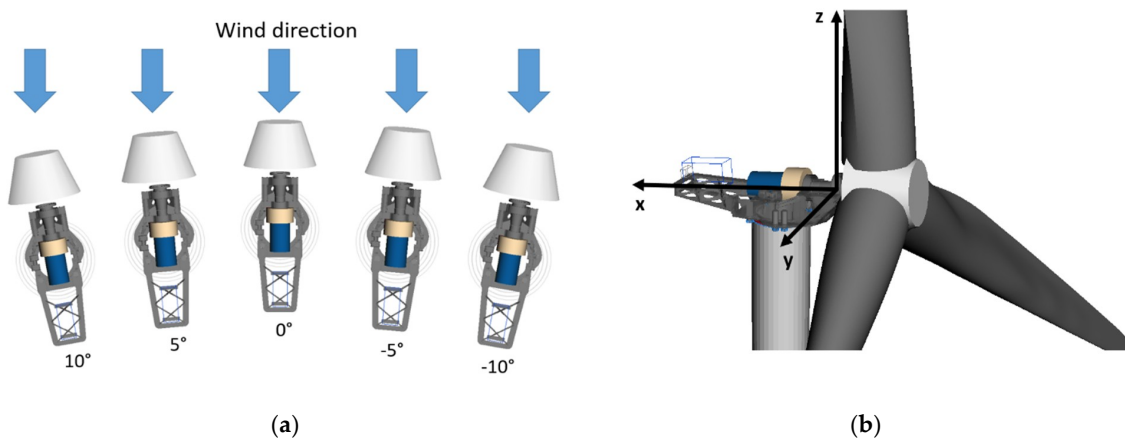


Figure 1. (a) Nacelle positions relative to wind direction as seen from above; (b) multi body simulation model of the C3 × 126 with coordinate system [15].

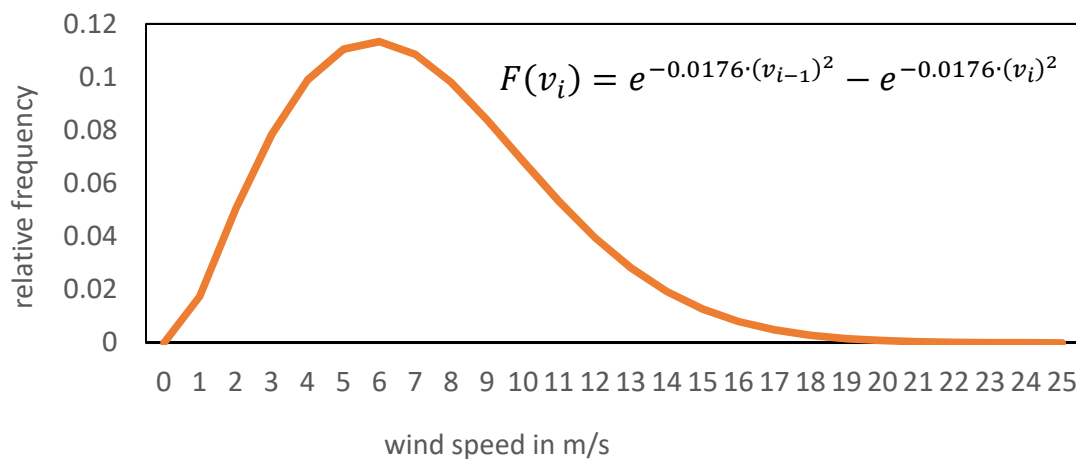


Figure 2. Relative frequencies of occurrence for various wind speeds used for load duration calculation.

3. Results and Discussion

The evaluation of the different inflow angles will be performed for five different yaw angles as mentioned before. Therefore six 10-min simulations with six different random seeds are carried out for each wind speed and each yaw misalignment. This results in a total number of 138 inflow simulations and 690 load simulations. To arrange the results in a compact and observable manner, load duration distributions are calculated in a first step. Building on this, rain flow counts are carried out which will be mainly discussed. To further condense the results, the damage equivalent load (DEL) is calculated with Equation (5) according to the industry standard DIN 50100 [21] for each yaw misalignment.

$$\text{DEL} = \sum S_i^k \cdot \left(\frac{N_i}{N_{eq}} \right)^{\frac{1}{k}}, \quad \text{with } k = 3.3 \quad (5)$$

This parameter is used to retrieve a force or torque for an equivalent load cycle where S_i the load of the corresponding load cycle is N_i . There $N_{eq} = 175,000$ load cycles are used, representative for a 20 year lifetime and an exponent of $k = 3.3$ as it is recommended for the lifetime calculation of bearings with a line contact in [22]. Afterwards, all combinations of load cycles and amplitudes can be summed up to one amplitude with an equivalent amount of load cycles.

In the following part of this work the loads are defined according to the hub coordinate system from Figure 1 (x-axis is coaxial with the shaft axis of rotation). The rain flow count diagrams, shown in Figures 3–5, contain relevant information about the load behaviour of the turbine and will be discussed.

A rain flow count is utilised to determine the number of load cycles from a load time series. The x- and y-axis represent the starting (x-axis) and ending (y-axis) load of the respective load cycle while the logarithmic colour scale gives the total number of load cycles of this type.

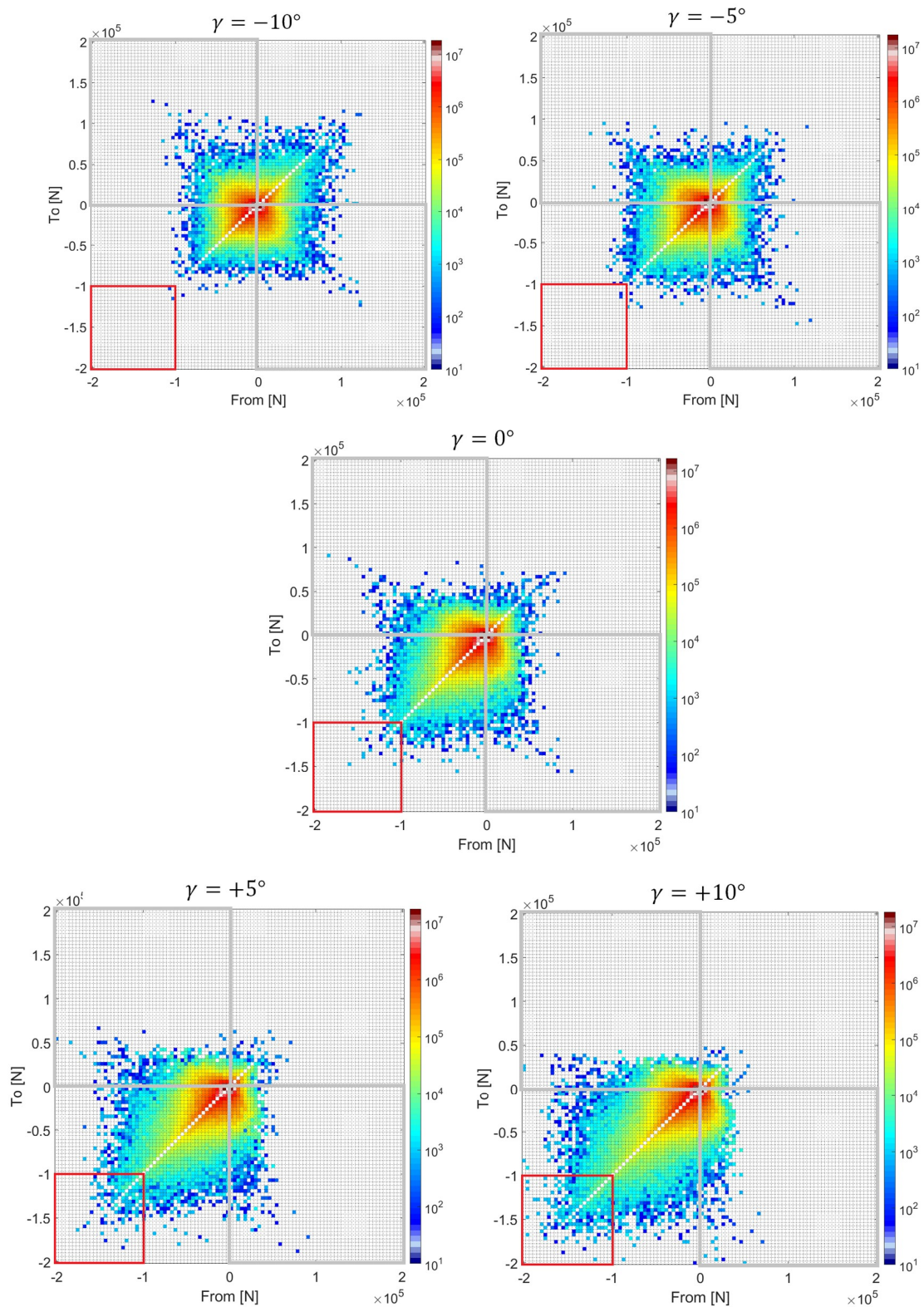


Figure 3. Rain flow count of the in-plane side force (y-axis) for various nacelle positions and a timespan of 20 years (top left: -10° ; top right: -5° ; middle: 0° ; bottom left: 5° ; bottom right: 10°).

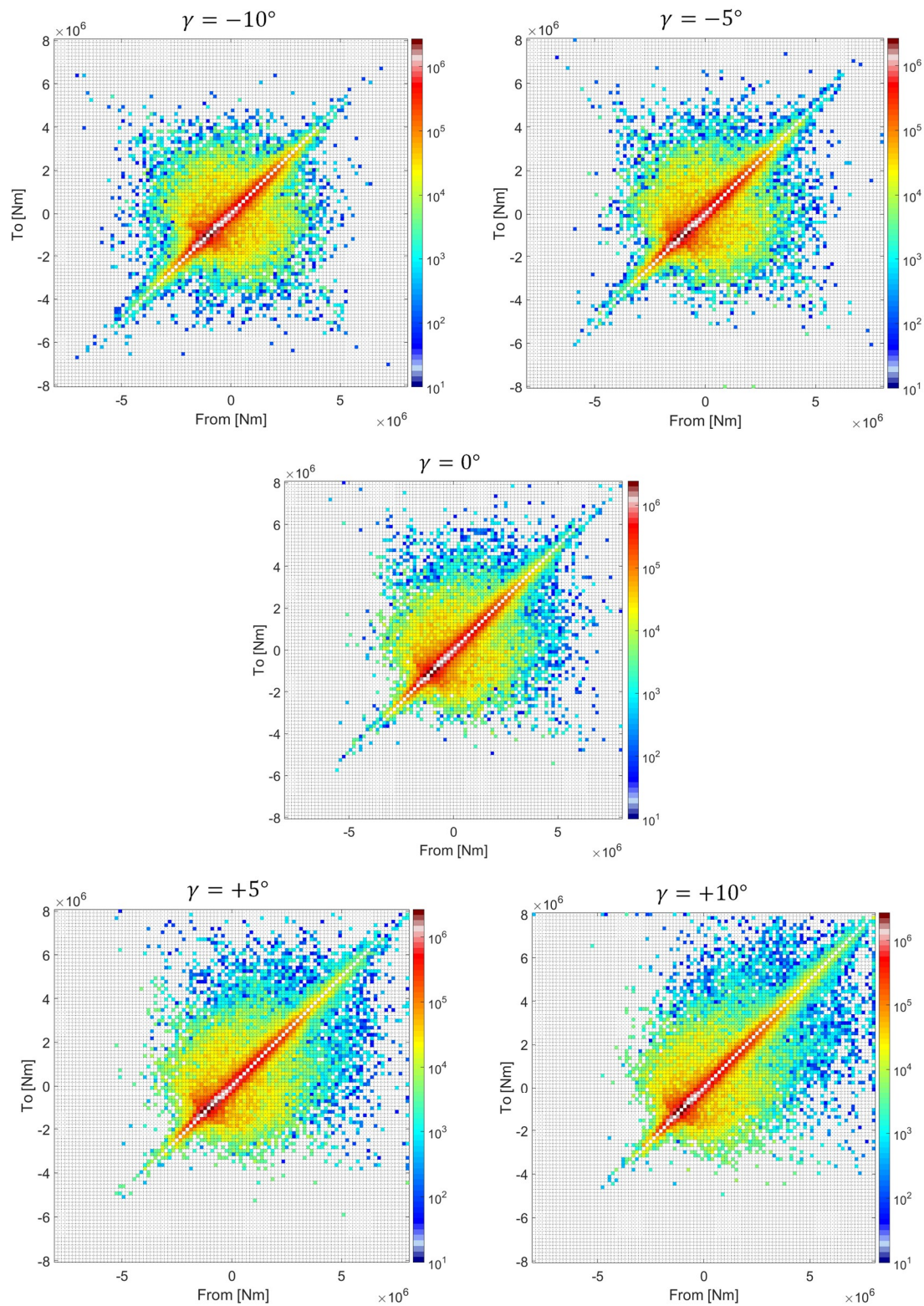


Figure 4. Rain flow count of the tilt moment (around y-axis) for various nacelle positions and a timespan of 20 years (top left: -10° ; top right: -5° ; middle: 0° ; bottom left: 5° ; bottom right: 10°).

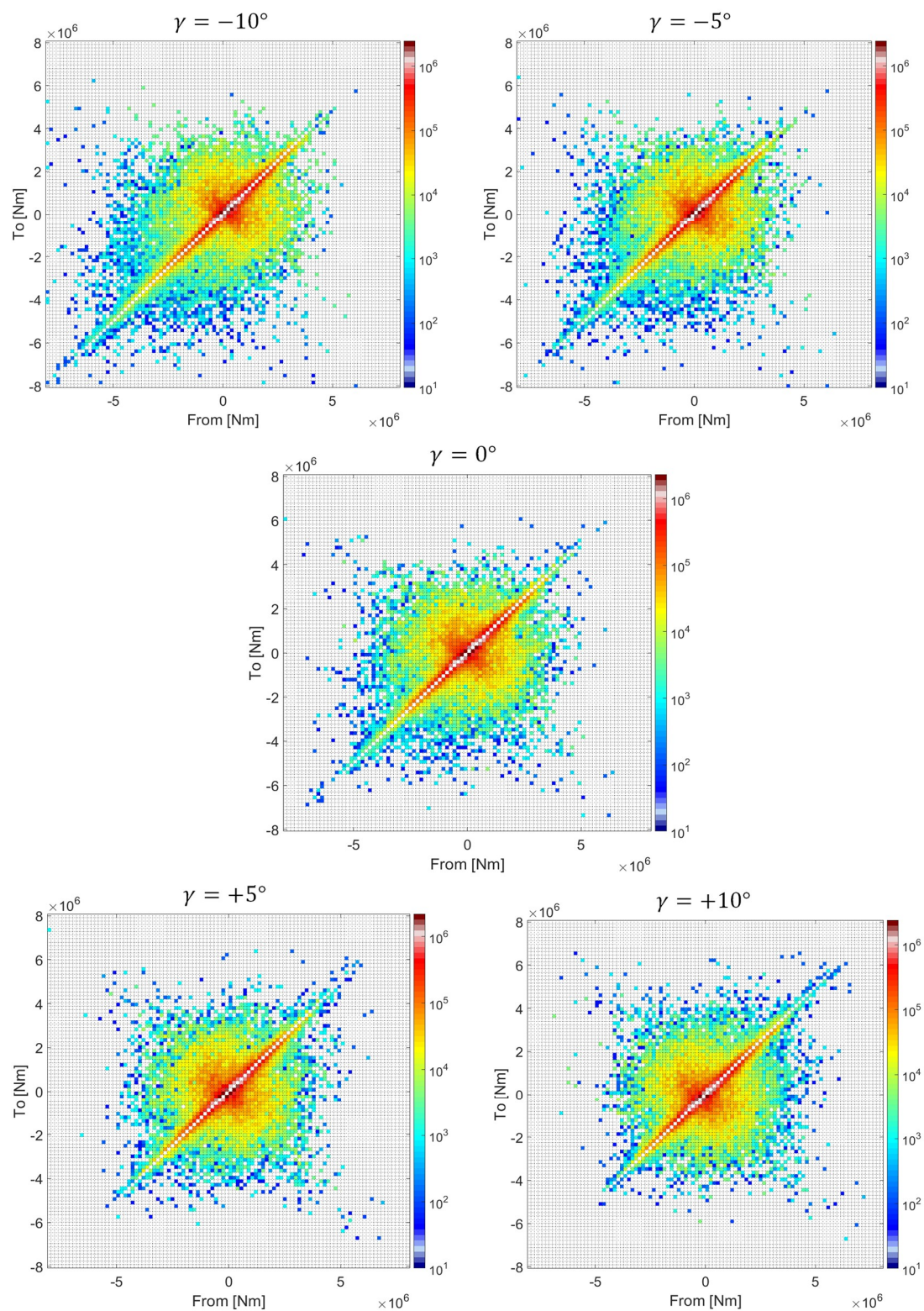


Figure 5. Rain flow count of the bending moment (around z-axis) for various nacelle positions and a timespan of 20 years (top left: -10° ; top right: -5° ; middle: 0° ; bottom left: 5° ; bottom right: 10°).

Rain flow count diagrams of the torsional torque as well as the axial force (x-axis) and the in-plane vertical force (z-axis) were analysed. The torsional torque and the axial force show no qualitative dependency on the yaw misalignment which matches the results from the literature [13].

The comparable small changes can be attributed to the reduced projected rotor area perpendicular to the inflow. In addition, the vertical in-plane force suffers only marginal changes because it is dominated by the rotor weight which is constant for all simulations.

The in-plane horizontal force is known to have one main direction resulting from the tangential forces acting on the rotor blades. The tangential forces on the blades point towards the rotational direction. However, in the upper half of the rotor they are greater due to the wind shear and the tower shadow leading to a horizontal force on the main bearing pointing to the right when looking downstream. When utilizing the coordinate system shown in Figure 1, the main direction of the side force is the negative y-direction. Figure 3 shows rain flow counts for the in-plane side force. It is observable that the changes are not only dependent on the absolute angle but on the sign as well. Negative angles evoke smaller maximum loads in the main direction. This can be well observed by comparing the load cycle numbers in the interval $[-2;-1;-2;-1]$ (red square). At the same time more load cycles with a changing force direction occur (load cycles in top left or bottom right quadrant, surrounded by grey squares). The tilt moment shows the same qualitative behaviour as the in-plane side force as it can be seen in the top right quadrants of Figure 4. Summarizing, this means that for the side force and bending moment the mean loads become greater with increasing angles but fewer zero-crossings occur. For the bending moment around the z-axis the previously observed effects are inverted (Figure 5). Smaller maximum loads, but more zero-crossings, occur with positive yaw misalignments.

Figure 6 shows the normalized damage equivalent loads for all six degrees of freedom and all yaw misalignments considered in this work. As found before the torsional moment, the axial force and the in-plane vertical force are not affected by yaw misalignments to the same extent as the other loads. As expected from the previous observations, the DEL of the in-plane side force (F_y) increases with the yaw angle. If the value at 0° is taken as a reference, the DEL decreases by -15.1% and increases by $+18.7\%$ in the investigated range. The same is true for the tilt moment (M_y) with a relative decrease of -1.2% for a -10° yaw misalignment and an increase of $+5.1\%$ for $+10^\circ$ yaw misalignment. Although the in-plane side force experiences the highest relative changes, its absolute values are comparably small to the other loads. The bending moment (M_z) shows a local minimum at 5° yaw angle. The DEL decreases slightly to -0.8% . A broader range of yaw misalignments would be necessary to observe if this is a global minimum. For a negative rotation the DEL is increased by $+8.1\%$ for -10° yaw angle.

To better understand these results one can look into the details of the aerodynamic coefficients that are used for calculating the aerodynamic forces. Figure 7 shows the lift and drag coefficients of the NACA64 airfoil taken from [23] which is used in the upper 33% of the blade length. The airfoils used in the rest of the blade differ only insignificantly from the NACA64. The effect of yaw misalignments on the local inflow at the blade elements can be derived from Figure 8. If the nacelle is rotated towards negative angles, the angle of attack decreases for the blade elements in the upper half of the rotor disk and increases for the blades in the lower half. This leads to a change of lift forces which results in a smaller in-plane side force at the main bearing. Conversely, the angle of attack in the upper half increases with a positive rotation of the nacelle, which leads to a greater side force. Similar observations can also be made for the tilt moment. It is mainly affected by the difference between the drag forces acting on the blades in the upper and in the lower half of the rotor disk. Rotating the nacelle in a negative direction will decrease the angle of attack in the upper half and increases it in the lower half. Thereby the difference of the drag forces becomes smaller. This finally leads to a smaller tilt moment at the main bearing. Again similar to the tilt moment, the bending moment is determined by the difference of the drag forces on the left and right rotor disk half. When rotating the nacelle against the inflow the projected wind speed as seen from the blade elements becomes smaller on both sides. This leads to a decrease of angle of attack on the right rotor half (blades that are moving towards the ground) when looking downstream and an increase of angle of attack on the left rotor half (blades that are moving upwards). This effect increases the difference between the drag forces and thus the

bending moment and it occurs for both directions of rotation. Therefore, the minimum that was found for the bending moment is very likely to be the global minimum on the basis of these conclusions.

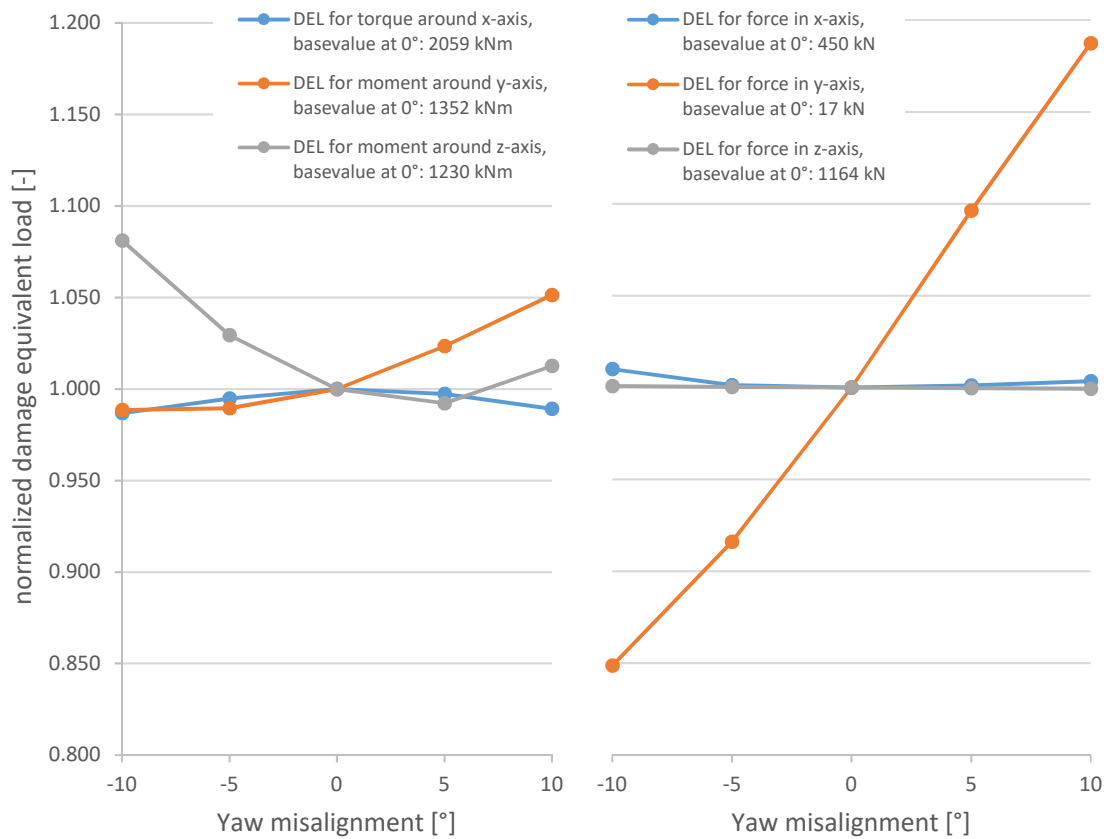


Figure 6. Damage equivalent load for the loads in all six degrees of freedom, various nacelle positions and a timespan of 20 years for an exponent of $k = 3.3$ (left: moments; right: forces).

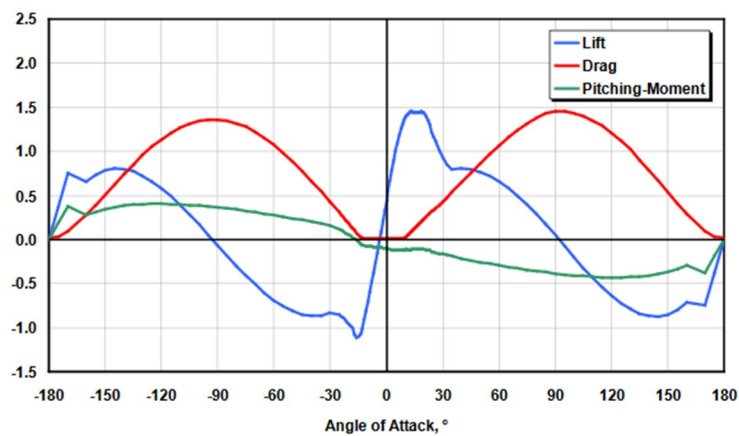


Figure 7. Coefficients of the NACA64 airfoil [23] shown as the respective dimensionless coefficient (y-axis) vs. angle of attack (x-axis).

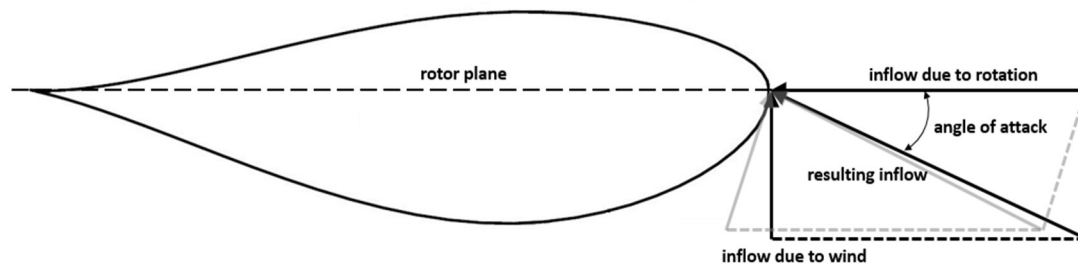


Figure 8. Schematic of the inflow conditions for a yaw misalignment of 0° (black lines) and a positive yaw misalignment (grey lines) for the blade elements of a blade at highest position.

It can be stated that the principle of wake steering offers good potential to increase the general park output as the literature shows. However, it is always to be taken into account that a possibly higher damage accumulation rate is a result. For validation of the real load distribution under wake steering in-field data of a steered turbine e.g., from condition monitoring is necessary.

4. Conclusions

The work carried out in this paper showed the effects of yaw misalignment on loads for a generic turbine. The active misalignment of turbines against the inflow direction is a tool to increase overall power output of the park as well as to decrease overall non-torque loads. However, the turbine that is misaligned itself will not necessarily benefit from this control scheme. A change in non-torque loads is to be expected. The influence of a yaw misalignment over a total timespan of 20 years is examined and analysed in this study. It is found that the differences in loads induced by yaw misalignments aren't symmetrical but dependent on the direction of the inflow. A clockwise rotation of the turbine, as seen from above, leads to smaller maximum loads as well as smaller average load cycle amplitudes for the horizontal in-plane force and the moment around the y-axis. If the turbine is rotated counter clockwise it shows the mentioned above effects for the moment around the z-axis up until 5° . Beyond that the effect seems to be reversed. It can be stated that wake steering does not necessarily have a negative impact on each drive train load, but the influence is to be taken into account. A basic understanding of the load behaviour due to wake steering is achieved. It is absolutely necessary to consider the non-torque-loads when implementing such a control scheme rather than solely focussing on the power output. In further studies, the load distributions calculated in this work can be merged with distributions of yaw misalignments due to wake steering to predict the load spectrum under real conditions. In addition, a cost function for weighting the various loads could be propagated to determine a preferential rotational direction when wake steering is necessary.

Author Contributions: M.C. and B.R. conceived and designed the experiments; M.C. performed the experiments; M.C. and B.R. analyzed the data; R.S. and G.J. contributed materials and analysis tools; M.C. wrote the paper.

Funding: This research was funded by VGB PowerTech.

Conflicts of Interest: The authors declare no conflict of interest.

References

1. Roscher, B.; Werkmeister, A.; Jacobs, G.; Schelenz, R. Modelling of Wind Turbine Loads nearby a Wind Farm. *J. Phys. Conf. Ser.* **2017**, *854*, 012038. [[CrossRef](#)]
2. Johnson, K.; Thomas, N. Wind farm control: Addressing the aerodynamic interaction among wind turbines. In Proceedings of the 2009 American Control Conference, St. Louis, MO, USA, 10–12 July 2009.
3. Park, J.; Kwon, S.; Law, K. Wind farm power maximization based on a cooperative static game approach. In Proceedings of the SPIE Active and Passive Smart Structures and Integrated Systems Conference, San Diego, CA, USA, 10 April 2013.

4. Gebraad, P.M.O.; Teeuwisse, F.W.; Van Wingerden, J.W.; Fleming, P.A.; Ruben, S.D.; Marden, J.R.; Pao, L.Y. Wind plant power optimization through yaw control using parametric model for wake effect—A CFD simulation study. *Wind Energy* **2014**, *19*, 95–114. [CrossRef]
5. Marden, J.R.; Ruben, S.D.; Pao, L.Y. A model-free approach to wind farm control using game theoretic methods. *IEEE Trans. Control Syst. Technol.* **2013**, *21*, 1207–1214. [CrossRef]
6. Fleming, P.; Gebraad, P.M.O.; Lee, S.; van Wingerden, J.W.; Johnson, K.; Churchfield, M.; Michalakes, J.; Spalart, P.; Moriarty, P. Simulation comparison of wake mitigation control strategies for a two-turbine case. *Wind Energy* **2015**, *18*, 2135–2143. [CrossRef]
7. Fleming, P.; Gebraad, P.; Lee, S.; van Wingerden, J.; Johnson, K.; Churchfield, M.; Michalakes, J.; Spalart, P.; Moriarty, P. Evaluating techniques for redirecting turbine wakes using SOWFA. *Renew. Energy* **2015**, *70*, 211–218.
8. Fleming, P.; Annoni, J.; Shah, J.J.; Wang, L.; Ananthan, S.; Zhang, Z.; Hutchings, K.; Wang, P.; Chen, W.; Chen, L. Field test of wake steering at an offshore wind farm. *Wind Energ. Sci.* **2017**, *2*, 229–239. [CrossRef]
9. Gebraad, P.; Thomas, J.; Ning, A.; Fleming, P.; Dykes, K. Maximization of the annual energy production of wind power plants by optimization of layout and yaw-based wake control. *Wind Energy* **2017**, *20*, 97–107. [CrossRef]
10. Gebraad, P.M.O. Data-driven wind plant control. Ph.D. Thesis, Delft University of Technology, Delft, The Netherlands, 2014.
11. Santoni, C.; Ciri, U.; Rotea, M.; Leonardi, S. Development of a high fidelity CFD code for wind farm control. In Proceedings of the 2015 American Control Conference (ACC), Chicago, IL, USA, 1–3 July 2015.
12. Ennis, B.L.; White, J.R.; Paquette, J.A. Wind turbine blade load characterization under yaw offset at the SWiFT facility. *J. Phys. Conf. Ser.* **2018**, *1037*, 052001. [CrossRef]
13. White, J.; Ennis, B.E.; Herges, T.G. Estimation of Rotor Loads Due to Wake Steering. In Proceedings of the 2018 Wind Energy Symposium, Kissimmee, FL, USA, 8–12 January 2018.
14. Lee, H.; Lee, D. Wake impact on aerodynamic characteristics of horizontal axis wind turbine under yawed flow conditions. *Renew. Energy* **2019**, *136*, 383–392. [CrossRef]
15. Werkmeister, A.; Schelenz, R.; Jacobs, G. Calculation of the design loads with SIMPACK, In Proceedings of the Simpack User Meeting Conference, Augsburg, Germany, 7 October 2015.
16. International Electrotechnical Commission (IEC). *Wind Turbines—Part 1: Design Requirements*, 3rd ed.; International Electrotechnical Commission (IEC): Geneva, Switzerland, 2014.
17. Zierath, J.; Rachholz, R.; Woernle, C. Field test validation of Flex5, MSC.Adams, alaska/Wind and SIMPACK for load calculations on wind turbines. *Wind Energy* **2016**, *19*, 1201–1222. [CrossRef]
18. Available online: <https://nwtc.nrel.gov/TurbSim> (accessed on 3 July 2019).
19. Moriarty, P.J.; Hansen, A.C. *AeroDyn Theory Manual*; Technical Report NREL/EL-500-36881; National Renewable Energy Laboratory: Golden, CO, USA, 2005.
20. International Electrotechnical Commission standard DIN 50100. *Load Controlled Fatigue Testing—Execution and Evaluation of Cyclic Tests at Constant Load Amplitudes on Metallic Specimens and Components*; Deutsches Institut für Normung E.V. (DIN): Pforzheim, Germany, 2016.
21. Renewable Energy Act of 21 July 2014 (BGBl. I S. 1066), last amended by Article 1 of the Act of 17 July 2017 (BGBl. I S. 2532). Available online: http://www.gesetze-im-internet.de/eeg_2014/EEG_2017.pdf (accessed on 9 May 2019).
22. Jacobs, G.; Corves, B. *Maschinengestaltung II*; Druck & Verlagshaus Mainz: Aachen, Germany, 2018.
23. Jonkman, J.; Butterfield, S.; Musial, W.; Scott, G. *Definition of a 5-MW Reference Wind Turbine for Offshore System Development*; Technical Report, No. NREL/TP-500-380060; National Renewable Energy Laboratory (NREL): Golden, CO, USA, 2009.

